Optical Fiber Technology 36 (2017) 6–9

Contents lists available at ScienceDirect

Optical Fiber Technology

www.elsevier.com/locate/yofte

Temperature-compensated refractive index sensor based on bent-fiber interference

Zhenfeng Gong, Ke Chen, Xinlei Zhou, Qingxu Yu *

School of Physics and Optoelectronic Technology, Dalian University of Technology, 2 Linggong Rd, Ganjingzi District, Dalian 116024, China

ARTICLE INFO

Article history:
Received 16 October 2016
Revised 16 January 2017
Accepted 29 January 2017

Keywords:
Single-mode fiber
Fiber Bragg grating
Fiber optics sensor
Interferometer

ABSTRACT

In this letter, we present a hybrid single-mode fiber (SMF) structure for refractive index (RI) measurement with the temperature compensation capability. The interferometer has simple structure, consisting of a bare fiber semicircular bending region (SBR) and a fiber Bragg grating (FBG). The section of SBR serves as a refractometer with a temperature compensator using a simple FBG. The sensing mechanism of this device has been investigated and experimentally demonstrated. The FBG structure is insensitive towards the change in the ambient RI but is sensitive towards the changes in the ambient temperature whereas the SBR structure is sensitive towards both of RI and temperature. In the RI range of 1.3288–1.3730, the corresponding RI sensitivity for the bare fiber bending region is 160 nm/RIU (refractive index unit) and the RI resolution is about 8.5×10^{-5} RIU.

1. Introduction

Fiber-optic refractive index (RI) sensors have been extensively investigated recently due to their special applications in biological and chemical industry, as well as their distinctive advantages over traditional RI sensors, such as miniature size, high sensitivity, and immunity to electromagnetic interference [1]. Some fiber-optic refractometers have been proposed in recent years, including optical fiber coil resonators [2], long period gratings [3], short period gratings [4], microfiber interferometer [5,6], multimode interferometer [7–11], silica-nanowire sensor [12], and photonic crystal fiber based refractive index sensors [13]. Some of these methods possess high RI sensitivities, but the sensors are unstable for practical applications. The sensing elements are typically brittle, and in addition, these methods usually involve special optical setup and bulky equipments, which increase complexity of fabrication and the cost. Most of the previously published investigations on bent fibers focused on reduction of bend loss, which is adverse for light transmission [14–16]. Recently, some researchers used bent fibers as optical sensing elements [17–22], which can be divided into two main types: intensity demodulated [18] and wavelength demodulated [19–22]. Especially, a C-shaped ultra-thin fiber RI sensor possessed a high RI sensitivity. Fiber stretching and ultra-thin fiber bending made up the C-shape bent fiber fabrication [19]. In [20], due to their low cost and simple fabrication process, Mach-Zehnder interferometer (MZI) based on S-like fiber tapers was proposed for sensing applications. However, the tapering process makes the sensor fabrication very complex. Previously, we proposed and demonstrated a dual-channel fiber-optic refractometer based on intermodal interference from single-mode fiber (SMF) bending. It has many distinctive advantages such as simple configuration, easy fabrication and ease of multiplexing. But the temperature-RI crosstalk is still an issue for refractive sensing [21].

In this letter, we propose a hybrid fiber structure as a temperature-compensated refractometer based on a FBG and a bare fiber SBR. The fiber-optic refractometer has many distinctive advantages over other RI sensors based on bending fiber [19–21], such as temperature compensation, easy fabrication and simple configuration. Experimental results show that the sensor has a high sensitivity of 160 nm/RIU versus the RIs of surrounding environment. Because the fabrication of the temperature-compensated fiber-optic interferometer is cost-effective and simple in comparison with other fiber-optic refractometers above-mentioned, it is a good sensor for RI measurement.

2. Sensor design and operating principle

The schematic diagram of the hybrid fiber structure is shown in Fig. 1. It consists of a FBG and a SBR. The left portion of Fig. 1 shows the SBR. The protective coating of the bending sections with 5 mm bending radius is stripped off. It will be conducive to the high interference interaction and visibility between the optical field and the surroundings. As shown in Fig. 1, when the core mode

* Corresponding author.
E-mail address: yuqx@dlut.edu.cn (Q. Yu).

http://dx.doi.org/10.1016/j.yofte.2017.01.011
1068-5200/

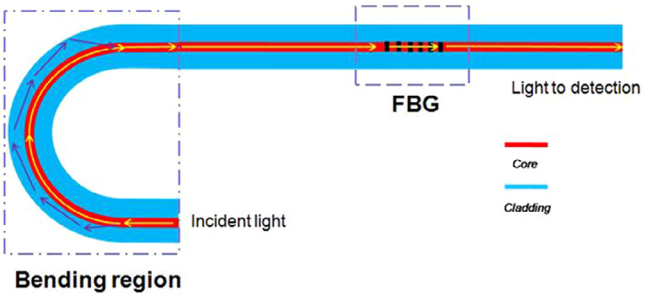

Fig. 1. Schematic diagram of temperature-compensated refractometer based on bent-fiber intermodal interference.

enters the SBR, the light power is split into two portions: firstly, the light is partially leaked into the cladding because of the bending, several cladding modes are excited and propagate along the fiber; secondly, the other light that is not leaked to the cladding continues to spread as the core mode. At the end of SBR, the cladding modes are coupled back to the core mode where interference occurs. It is known that the RIs of the surrounding medium will affect the RIs of the cladding modes, so the transmission spectrum changes as the surrounding RI changes. A FBG is then spliced to the output end of the SBR.

For the FBG, it is known that the resonance wavelength of FBG will not shift as the surrounding RI changes. For the SBR, after propagating through a SBR with a selected bending radius R, the phase difference between the core and the ath-order cladding mode can be written as:

$$\Delta\phi_a = \frac{2\pi}{\lambda}\left(n_{core,eff} - n_{clad,a,eff}\right)l = \frac{2\pi}{\lambda}\Delta n_{eff}\pi R = (2k+1)\pi \tag{1}$$

Where $n_{core,eff}$ and $n_{clad,a,eff}$ are the effective RIs of the core mode and the ath-order cladding mode, respectively. l is the length of SBR, λ is the wavelength of the transmission dip, $\Delta n_{eff} = n_{core,eff} - n_{clad,a,eff}$ is the effective RI difference between the core mode and the ath-order cladding mode, and k is an integer. Constructive or destructive interference will occur because of the phase difference between the core mode and cladding modes. Since the effective RI of the cladding mode is related to the surrounding RI, the transmission dip wavelength of SBR will shift when the sensor is subjected to surrounding RI perturbation. External RI changes can be detected and evaluated through the resonance wavelength shift. We can deduce the sensitivity of the transmission dip of SBR to the change of surrounding RIs from Eq. (1) as:

$$\frac{d\lambda}{dn} = \frac{-\lambda}{\Delta n_{eff}}\frac{\partial n_{clad,a,eff}}{\partial n}\Bigg/\left[1 - \frac{\lambda}{\Delta n_{eff}}\left(\frac{\partial n_{core,eff}}{\partial \lambda} - \frac{\partial n_{clad,a,eff}}{\partial \lambda}\right)\right] \tag{2}$$

3. Experiments and discussions

A commercial standard SMF (Coning, SMF-28) is used to fabricate the designed sensor. In the experimental setup, a homemade optical sensing interrogator with a spectral resolution of 4 pm is used to measure the transmission spectrum of the structure. A swept laser provides an output wavelength range from 1510 nm to 1590 nm. The peak power output of the light source is 5 mw. The transmitted light signal is detected by the photoelectric converter in the optical sensing interrogator (OSI), demodulated by a data acquisition unit and software, and then the spectra signal is displayed on a computer. The transmission spectra of the structure are shown in Fig. 2(a). We investigate the spectra of the SBR with different bending radiuses in order to understand the influence of the bending radius on the optical spectra. In Fig. 2(b), there is an obvious dip located at 1567.0 nm with 4 mm bending radius. Fig. 2(c) shows an interference dip at 1572.5 nm with 5 mm bending radius. The dotted red lines in Fig. 2(b) and (c) are the repeatable spectra. The positions of the interference dips are repeatable. We select the SBR with the radius of 5 mm which functions as the interferometer in our experiment, because it is more durable. The grating period of the FBG used in our experiment is 532.5 nm and the resonant valley of the FBG is located at about 1542 nm. An inset of Fig. 2(a) shows the spatial spectra of dip 2; from the inset, it is known that the mode coupling and interference mainly occur between the core mode and the single dominant higher-order mode.

The RI sensing of the fiber-optic temperature-compensated refractometer with the 5 mm bending radius of SBR and 18 dB resonance depth of FBG is experimentally investigated. A polymethyl methacrylate plate is used as the platform and the SBR is bound on it. Different concentrations of sodium chloride (NaCl) solutions are acted as surrounding RI samples. The temperature of NaCl solutions is maintained at 20 °C. The structure is cleaned with ethanol and dried to recover its original spectrum after every experiment. The RI responses of the sensor are shown in Fig. 3. In Fig. 3(a), there are two evident dips named as Dip 1 and Dip 2, respectively, formed by the FBG and SBR. Fig. 3(b) and (c) show enlarged figures of dip 1 and dip 2, respectively. From Fig. 3(c) we know that, as the surrounding RI increases from 1.3328 to 1.3730, the dip 2 wavelength shifts towards to the longer wavelength. Fig. 3(b) shows that the resonance wavelength of FBG is almost unchanged.

The inset of Fig. 3(a) presents the wavelength of the spectral dips as a function of the RIs. From the linear fit, the RI sensitivity of the SBR is 160 nm/RIU and the RI resolution is about 8.5×10^{-5} - RIU, while the central wavelength of FBG remains relatively motionless.

In practical applications, temperature cross-sensitivity is an important issue for many RI sensors, so we also investigate the temperature response of the structure. The structure is mounted on a glass plate immersed into the deionized water. The liquid temperature is increased gradually from 30 °C to 50 °C, with a temperature interval of 1 °C. Fig. 4 presents the transmission spectra versus temperature. As shown in Fig. 4, the dip 1 and dip 2 move with the temperature. Fig. 4(b) and (c) are enlarged figures of dip 1 and dip 2, respectively. The temperature responses are shown in the inset of Fig. 4(a). When the liquid temperature increases gradually, the resonance wavelength of the FBG moves towards to longer wavelength and the resonance wavelength of the SBR moves towards to shorter wavelength, giving average temperature sensitivities of 4.6 pm/°C and −85.6 pm/°C for dip 1 and dip 2, respectively.

Fig. 5 shows the characteristic responses of the sensor when subjected individually to different ambient temperatures and refractive indices, respectively. For the RI sensing, the sensor is immersed in different concentrations of NaCl solutions to achieve different ambient refractive indices. For the temperature sensing, the device is kept mounting on a glass plate immersed into the deionized water and the temperature is increased from 30 °C to 50 °C. The response is measured in terms of the corresponding wavelength shifts observed for the valleys in the spectra of FBG and SBR, respectively.

It is observed that the FBG is sensitive to the temperature only, while the SBR is sensitive to both the temperature and surrounding RIs. Therefore, the FBG structure can be used as a temperature compensator during the RI measurement. In Fig. 5, it is known that the temperature sensitivities of the FBG and SBR are drastically different. The reason is that the high cladding mode of the SBR is much more sensitive to the material properties change.